Acta Biochim Biophys Sin 2012, 44: 737–745 | © The Author 2012. Published by ABBS Editorial Office in association with Oxford University Press on behalf of the Institute of Biochemistry and Cell Biology, Shanghai Institutes for Biological Sciences, Chinese Academy of Sciences. DOI: 10.1093/abbs/gms060.
Advance Access Publication 25 July 2012

Original Article

Interferon-β-armed oncolytic adenovirus induces both apoptosis and necroptosis in cancer cells

Hongling Huang[1†], Tian Xiao[1†], Lingfeng He[3], Hongbin Ji[1*], and Xin-Yuan Liu[1,2*]

[1]State Key Laboratory of Cell Biology, Institute of Biochemistry and Cell Biology, Shanghai Institutes for Biological Sciences, Chinese Academy of Sciences, Shanghai 200031, China
[2]Xinyuan Institute of Medicine and Biotechnology, Zhejiang Sci-Tech University, Hangzhou 310018, China
[3]Department of Medicine, Beth Israel and Deaconess Medical Center, Harvard Medical School, Boston, MA 02215, USA
[†]These authors contributed equally to this work.
*Correspondence address. Tel/Fax: +86-21-54921126; E-mail: xyliu@sibs.ac.cn (X.L.)/Tel: +86-21-54921108; Fax: +86-21-54921101; E-mail: hbji@sibs.ac.cn (H.J.)

Interferon-β (IFN-β) has been widely used in cancer therapy, but the clinical trial results are generally disappointing. Our previous studies have shown that an oncolytic adenovirus carrying IFN-β (ZD55-IFN-β) exhibits significant anti-tumor activities. However, the underlying mechanisms are not clear. Here we showed that ZD55-IFN-β infection-induced S-phase cell cycle arrest in a p53-dependent manner by activating the ataxia telangiectasia mutated-dependent DNA damage pathway. In addition, ZD55-IFN-β infection could initiate both caspase-dependent apoptosis and necroptosis in cancer cells. More importantly, ZD55-IFN-β showed a synergistic effect on cancer cells when combined with doxorubicin. These results suggest that the combination of ZD55-IFN-β with doxorubicin may represent a promising clinical strategy in cancer therapy.

Keywords IFN-β; cell cycle arrest; apoptosis; necroptosis; synergism

Received: April 5, 2012 Accepted: May 15, 2012

Introduction

Interferons (IFNs), which are naturally produced and released by lymphocytes in response to pathogens, belong to the large class of glycoproteins known as cytokines [1]. IFN-β is classified as a type I IFN and shows anti-proliferative effects in a number of cancer cell lines by inducing cell cycle arrest and apoptosis [2,3]. However, the detailed signaling pathways involved in IFN-β-induced cell cycle inhibition and apoptosis are not clear. IFN-β can also exhibit indirect anti-tumor effects through immune stimulation [4] and anti-angiogenic properties [5]. As an agent used in gene therapy, IFN-β can inhibit tumor formation and cancer metastasis in various malignancies of animal models [6]. Clinical trials with recombinant IFN-β have also been performed [7], but the results were not satisfied. Our previous study has shown that an oncolytic adenovirus carrying IFN-β (ZD55-IFN-β) exhibits significant anti-tumor activities [8]. However, the underlying mechanisms are not clear.

Drug resistance is a major problem in cancer chemotherapy, which could contribute to recurrence of disease or even death [9]. Since defects in apoptosis signaling are a major cause of drug resistance, current approaches attempt to restore the efficacy of chemotherapy by reactivating apoptosis are particularly difficult. It has been reported that cancer cells resistant to apoptotic inducers are sensitive to necroptosis [10]. Therefore, overcoming cancer drug resistance might be achievable by simultaneously activating both apoptosis and necroptosis [11]. Necroptosis is a kind of programmed necrotic cell death that can be identified by cell morphology (necrosis), loss of membrane integrity and mitochondrial membrane potential, subsequent ATP depletion, and LC3-II accumulation [12]. Like apoptosis, necroptosis is executed by regulated mechanisms. It is dependent on the serine/threonine kinase activity of receptor interacting protein 1 (RIP-1), which is inhibited by a specific molecule, necrostain-1 (Nec-1). Necroptosis has been found to contribute to delayed injury in mouse models of ischemic brain injury [13], and it also plays a role in the cell death induced by some chemical drugs [14,15].

Here, we report that, in addition to inducing apoptosis, IFN-β-armed oncolytic adenovirus (ZD55-IFN-β) promoted cell cycle arrest and necroptosis. Moreover, ZD55-IFN-β had a synergistic effect on cancer cells when combined with doxorubicin, indicating the strong potential of ZD55-IFN-β to reverse cancer drug resistance. These findings suggest a

promising clinical anti-tumor strategy through administration of ZD55-IFN-β.

Materials and Methods

Antibodies and reagents

Anti-caspase-9, anti-caspase-3 and anti-β-actin antibodies, horseradish peroxidase (HRP)-conjugated secondary antibodies were purchased from Santa Cruz Biotechnology (Santa Cruz, USA). Phospho-ataxia telangiectasia mutated (ATM) (Ser1981), phospho-Chk2 (Thr68), cleaved caspase-3 antibodies were from Cell Signaling Technology (Beverly, USA). The antibody for LC3 was purchased from MBL International (Woburn, USA). The pan-caspase inhibitor, Z-VAD-FMK, and necroptosis inhibitor, Nec-1, were purchased from Alexis Biochemicals (San Diego, USA). Propidium iodide (PI), doxorubicin, caffeine, 3-(4, 5-dimethylthiazol-2-yl)-2, 5-diphenyltetrazolium bromide (MTT), and a JC-1 fluorescent probe were purchased from Sigma (St Louis, USA). 4′,6-diamidino-2-phenylindole (DAPI) was purchased from Beyotime (Nanjing, China).

Cell culture

Human hepatoma cell line SMMC-7721, Hep-3B, human breast adenocarcinoma cell line MCF-7, MDA-MB-231, and human embryonic kidney cell line HEK293 were maintained in Dulbecco's modified Eagle's medium (DMEM; GIBCO, Carlsbad, USA) supplemented with 10% heat-inactivated fetal bovine serum (FBS; GIBCO), 100 U/ml of penicillin, and 100 mg/ml of streptomycin. NCI-H358 and DU-145 cells were grown in RPMI 1640 medium (GIBCO) containing 10% FBS, penicillin (100 U/ml), and streptomycin (100 U/ml).

Generation, identification, purification, and titration of adenovirus

The generation, identification, and purification of the conditionally replicative adenovirus carrying interferon-β (ZD55-IFN-β) were performed as described previously [8]. Briefly, pZD55-IFN-β was constructed, and then recombined with pBHGE3 (Microbix Biosystems, Ontario, Canada) in HEK293 cells for packaging the virus. The virus was identified by polymerase chain reaction (PCR). The titration of the adenovirus was determined by standard TCID50 method using HEK293 cells.

Real-time PCR analysis

Total RNA from cells was prepared using Trizol reagent (Invitrogen, Carlsbad, USA). A pool of single-strand cDNAs for PCR template was synthesized from 5 μg of total RNA using oligo(dT)$_{18}$ primer and RevertAid^{TM} First Strand cDNA Synthesis Kit (Fermentas, Burlington, Canada). The SYBR Green Real-time PCR Master Mix (TOYOBO, Osaka, Japan) was used for the subsequent PCR amplification. *GAPDH* mRNA was used to normalize RNA inputs. Primers used to amplify *p21* and *GAPDH* are available for request. The amplification efficiencies of all primers used here are between 95% and 105%.

Western blot analysis

Cells were harvested at different time points post-infection and resuspended in cell lysis buffer (Beyotime). Protein concentrations were determined by enhanced BCA protein assay kit (Beyotime), and then western blots were carried out using standard procedures. Briefly, 40 μg of the cellular proteins were separated by 12% sodium dodecyl sulfate polyacrylamide gels, and then transferred to Hybond-P polyvinylidene difluoride membranes (Millipore, Billerica, USA) followed by blocking with 5% non-fat milk in Tris-buffered saline-0.1% Tween-20 (TBST) for 1 h at room temperature (RT). The membranes were probed with indicated primary antibodies for 2 h at RT. After washed three times with TBST, the membranes were incubated with HRP-conjugated secondly antibodies for another 1 h followed by washing three times with TBST, and then developed by enhanced chemiluminescence according to the manufacturer's instructions (Pierce, Rockford, USA).

Cell viability assay

The cytotoxicities of ZD55-IFN-β, doxorubicin, and the combination of ZD55-IFN-β and doxorubicin were determined using the MTT assay, as described previously [8]. Briefly, cells were cultured in 96-well plates and followed by various treatments. At indicated time points, cell culture medium was removed, and relative cell numbers were investigated by incubating cells with MTT for 4 h. The resultant formazan was dissolved in dimethyl sulfoxide and the absorbance was measured at 490 nm. Cell viability was calculated as the absorbance in treated cells divided by the absorbance in control cells.

Combination index and improved IC_{50}-isobologram analysis for determining synergism and antagonism

The methods used for improved IC_{50}-isobologram and combination index (CI) analyses have been described by Aoe *et al*. [16]. For CI analysis, CalcuSyn V2.0 was used to calculate IC_{50} value and CI based on dose−response curves. $CI < 1$, $CI = 1$ and $CI > 1$ represented synergism, additive, and antagonism, respectively. For improved IC_{50}-isobologram analysis, an 'envelope of additivity' was enclosed by three isoeffect curves (modes I, IIA, and IIB). When the experimental IC_{50} data points for the combination plotted below the envelope, the combination of the two drugs was supra-additive (synergism). When the experimental IC_{50}

data points for the combination were within the envelope, the combination was regarded as additive. When the experimental IC_{50} data points for the combination were above the envelope, the combination was subadditive (antagonism).

Flow cytometry analysis

For PI exclusion, cells were harvested and stained with 5 μg/ml PI and immediately analyzed using a FACSCalibur (BD Bioscience, San Diego, USA). FL3-positive cells were identified as nonviable. For analyzing cell cycle and sub-G1 populations, cells were fixed in 70% ethanol and then stained with 50 μg/ml PI. To determine cells with low mitochondrial membrane potential, cells were stained with 2.5 μg/ml JC-1 and analyzed. Loss of red and increase in green fluorescence indicated loss of mitochondrial membrane potential. For reactive oxygen species (ROS) detection, 7721 cells with or without virus treatment were harvested, and resuspended in phosphate-buffered saline (PBS) containing 10 μM CM-H2DCFDA (Sigma). Cells were maintained at 37°C in the dark for 30 min, and then analyzed by flow cytometry.

Analysis of cell death

SMMC-7721 cells were pre-treated with or without 10 μM Nec-1. At different time points, cells were harvested and subjected to the PI exclusion assay. The necrotic cell death was distinguished from apoptotic cell death using Vitale's principle [17–19]. Necrotic cells take up PI quickly because of their extensive membrane damage, whereas apoptotic cells have much slower uptake of PI. Thus, healthy (PI-negative), apoptotic (PI-dim) and necrotic (PI-bright) cells were readily distinguished from each other.

To further distinguish necrotic cell death from apoptotic cell death, the cells stained with PI were analyzed by fluorescence microscopy (IX-71, Olympus, Tokyo, Japan) as reported previously [20]. The cells exhibiting fragmented nuclei were regarded as apoptotic, and the round cells were considered to be undergoing necrotic cell death. Ten microscopic fields and more than five hundred cells were examined in each sample.

Reporter gene assay

Reporter gene assay was carried out using Dual Luciferase Assay System (Promega, Madison, USA). Briefly, cells were transfected with p53-responsive *firely* luciferase construct and pRL-TK *Renilla* luciferase. And then the cells were infected with ZD55-EGFP or ZD55-IFN-β. At indicated time points, cells were harvested and the activities of *firely* luciferase and *Renilla* luciferase were determined by Promega GloMax® 20/20 Luminometer.

Immunofluorescence staining

Cells treated with ZD55-IFN-β or ZD55-EGFP were washed with PBS buffer and fixed by 4% formaldehyde for 10 min followed by penetration with PBS-0.4%Triton-X-100 (PBST) for another 10 min. And then cells were incubated with anti-cleaved caspase-3 (1 : 100) for 2 h at RT. After washed three times with PBST, the cells were incubated by fluorescein-conjugated secondary antibody for 45 min followed by washing and mounting. The image was scanned at confocal laser scanning microscopy (LeicaSP5, Wetzlar, Germany).

Statistical analysis

All data were expressed as the mean ± standard deviation (SD) and analyzed using Student's *t*-test by R statistics package (2.9.0). Results were considered statistically significant when $P < 0.05$.

Results

ZD55-IFN-β induces S-phase arrest in a p53-dependent manner

To systematically investigate the mechanism of anti-tumor activity of ZD55-IFN-β, we first determined its effect on regulating cell cycle progression. The results showed that the percentage of SMMC-7721 cells in S-phase dramatically increased from ~23.00% to 41.74% and 51.87% at 24 and 48 h after ZD55-IFN-β infection, respectively [**Fig. 1(A,B)**], which was accompanied by the up-regulation of *p21* at mRNA level [**Fig. 1(C)**]. Obvious S-phase arrest was also observed in ZD55-IFN-β-infected MDA-MB-231 and MCF-7 cells (**Table 1** and **Supplementary Fig. S1**), whereas ZD55-IFN-β treatment was incapable of inducing S-phase arrest in the two p53-null cell lines: NCI-H358 and Hep-3B (**Table 1**). Using a p53-responsive reporter construct, it was found that the p53 transcriptional activities were significantly increased at 24 and 48 h after ZD55-IFN-β infection in SMMC-7721 cells, indicating the activation of p53 in ZD55-IFN-β-induced S-phase arrest [**Fig. 1(D,E)**].

ZD55-IFN-β induces S-phase arrest by activating the ATM-dependent DNA damage pathway

S-phase arrest can be induced by many drugs through different signaling pathways [21,22], one of which is the DNA damage pathway, which sensing DNA damage through activating ATM/ATR(ATM-related)-Chk1/Chk2 kinase cascade [23]. Strikingly, we found that when cells were pre-treated with caffeine, an inhibitor of ATM and ATR kinase activities [24], the cell cycle arrest induced by ZD55-IFN-β was completely abolished [**Fig. 1(A,B)**]. Consistent with this result, western blot results showed that ZD55-IFN-β infection increased the level of the p-ATM

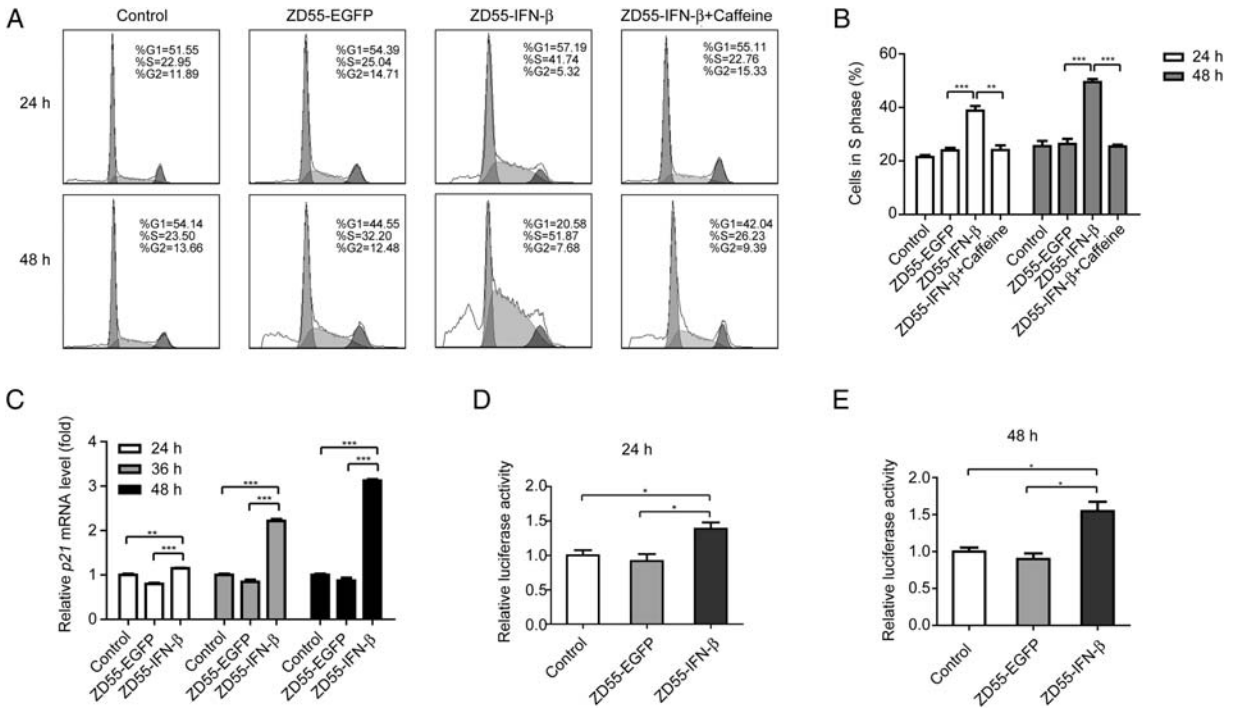

Figure 1 ZD55-IFN-β induces S-phase arrest in a p53-dependent manner (A) Cell cycle distribution in SMMC-7721 cells after various treatments. The percentage of cells in each phase is shown in the upper right. (B) Quantification of the S-phase population. (C) Real-time PCR analysis of the fold changes of *p21* mRNA. *GAPDH* mRNA was used as an internal control. The mRNA level of uninfected cells was used as a reference value. (D, E) Reporter gene assay using a p53-responsive construct in SMMC-7721 cells. Cells were infected with ZD55-EGFP or ZD55-IFN-β at MOI = 2. After 24 h (D) and 48 h (E), the *firely* luciferase activities were determined. pRL-TK was used as internal control. Results are expressed as the mean ± SD from three replicates. $*P < 0.05$, $**P < 0.01$, $***P < 0.001$.

Table 1 ZD55-IFN-β induces S-phase arrest in a p53-dependent manner

Human cancer cell lines	p53 status	Treatment (MOI = 2)	Cells in S phase (%)
MCF-7	WT	Control	23.78 ± 0.66
		ZD55-EGFP	23.41 ± 4.77
		ZD55-IFN-β	41.31 ± 1.64**
MDA-MB-231	Mutant	Control	10.82 ± 1.84
		ZD55-EGFP	9.25 ± 0.38
		ZD55-IFN-β	24.29 ± 1.17**
NCI-H358	Null	Control	18.01 ± 1.39
		ZD55-EGFP	20.01 ± 2.28
		ZD55-IFN-β	21.43 ± 0.22
Hep-3B	Null	Control	21.45 ± 1.19
		ZD55-EGFP	27.99 ± 1.23
		ZD55-IFN-β	25.24 ± 2.25

Notes: ZD55-IFN-β infection induced S-phase arrest in MCF-7 and MDA-MB-231 cells ($**P < 0.01$). But in NCI-H358 and Hep-3B cells, ZD55-IFN-β infection did not result in S-phase arrest ($P > 0.05$).

and p-Chk2 in SMMC-7721 cells, whereas caffeine could suppressed this elevation [**Fig. 2(A–C)**]. These data indicated that ZD55-IFN-β activated the ATM-dependent DNA damage pathway.

ZD55-IFN-β triggers apoptotic cell death in tumor cells

To validate the pro-apoptotic function of ZD55-IFN-β in tumor cells, the human hepatoma cells SMMC-7721 were infected with ZD55-IFN-β or a control virus (ZD55-EGFP) and submitted to sub-G1 analysis. As expected, the percentage of cells infected with ZD55-IFN-β in sub-G1 was markedly higher than that of ZD55-EGFP-infected cells [**Fig. 3(A)**]. ZD55-IFN-β infection also efficiently led to the cleavage of procaspase-9, procaspase-3 when compared with ZD55-EGFP [**Fig. 3(B–D)**]. Besides, when cells were pre-treated with Z-VAD-FMK, the increased proportion of cells in sub-G1 was restored [**Fig. 3(A)**]. These findings indicated that caspase-dependent apoptosis contributes to ZD55-IFN-β-induced cell death.

ZD55-IFN-β induces necroptosis in tumor cells

It has been reported that some drugs can achieve their therapeutic effect by inducing multiple types of cell death [14,25]. Herein, to comprehensively assess the anti-tumor mechanism of ZD55-IFN-β, several assays related to necroptosis were performed. Fluorescence-activated cell sorting analysis showed that, compared with the ZD55 vector, ZD55-IFN-β infection notably increased the percentage of cells with low mitochondrial membrane potential (MMP), suggesting that ZD55-IFN-β promotes MMP

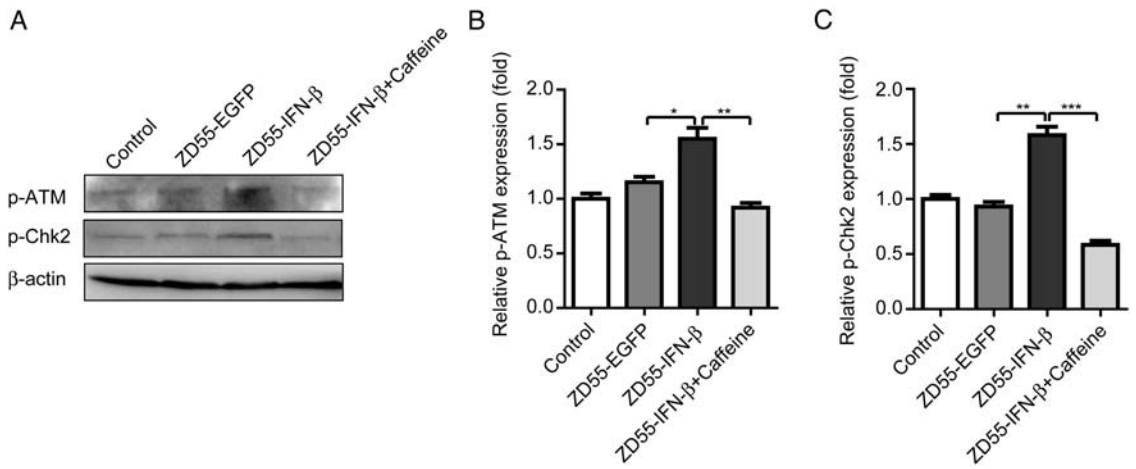

Figure 2 ZD55-IFN-β induces S-phase arrest by activating the ATM-dependent DNA damage pathway (A) Western blot analysis of DNA damage pathway-related proteins in SMMC-7721 cells infected with ZD55-EGFP or ZD55-IFN-β at MOI = 2. Caffeine (10 mM) was used as an inhibitor of ATM. β-actin served as a loading control. (B–C) The expression of p-ATM (B) and p-Chk2 (C) were quantified by densitometry and normalized by β-actin. Results are expressed as the mean ± SD from three separate experiments. $^{*}P < 0.05$, $^{**}P < 0.01$, $^{***}P < 0.001$.

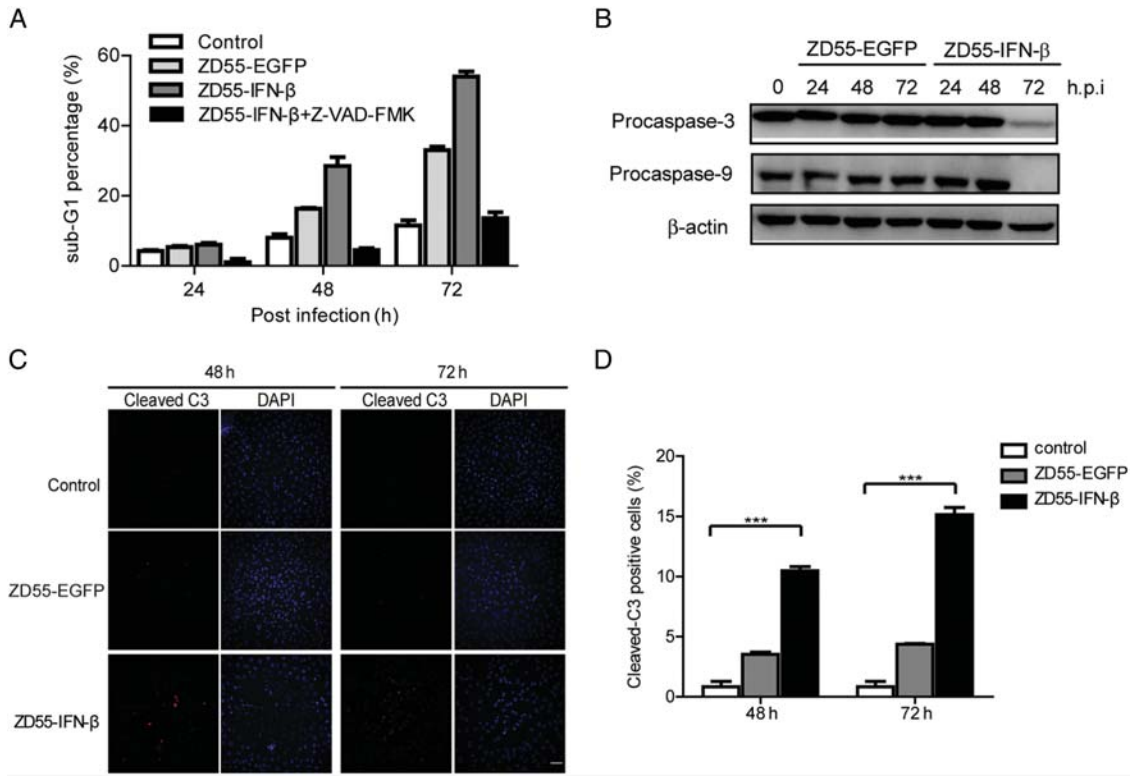

Figure 3 ZD55-IFN-β triggers apoptotic cell death (A) Quantification of the sub-G1 population after various treatments in SMMC-7721 cells. Z-VAD-FMK (25 μM) was used as the caspase inhibitor. (B) Western blot analysis of apoptosis-related proteins in SMMC-7721 cells after various treatments. h.p.i., hours post-infection. (C) Immunofluorescence staining of cleaved caspase-3 (red) in SMMC-7721 cells infected with ZD55-EGFP or ZD55-IFN-β at 48 and 72 h post-infection. MOI = 2. Nuclei were stained with DAPI. Scale bar = 100 μm. (D) Statistical analysis of the percentage of cleaved caspase-3 positive cells. Cells were calculated in 10 random fields at 200× from five separate slides per group. Results are expressed as the mean ± SD. $^{***}P < 0.001$.

loss in cancer cells [**Fig. 4(A)**]. When cells undergo necrotic cell death, the cellular ATP levels drop, but this phenomenon does not occur in cells undergoing apoptotic cell death [26]. At 24 h after ZD55-IFN-β infection, the cellular ATP levels dropped sharply and pre-treatment with Nec-1 could efficiently rescued the ATP levels [**Fig. 4(B)**] as well as improved the percentage of living cells by inhibiting the necrotic cell death [**Fig. 4(C)**], which

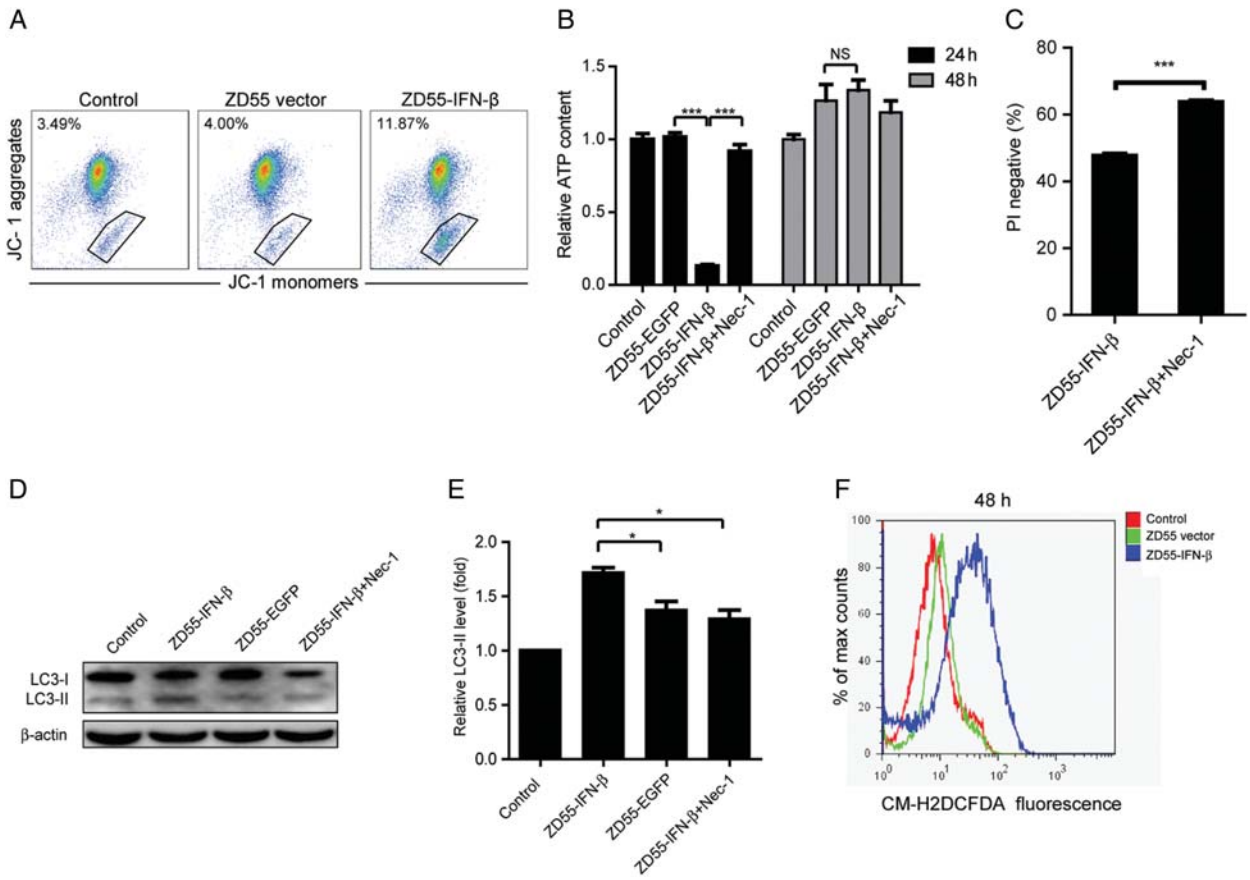

Figure 4 ZD55-IFN-β induces necroptotic cell death (A) Analysis of the MMP of SMMC-7721 cells. Cells with low MMP are outlined by solid lines, and the percentage is shown in the upper left. (B) Measurement of intracellular ATP in SMMC-7721 cells under different treatments. (C) Measurement of cell viability by PI exclusion assay. (D) Western blot analysis of LC3-II accumulation in SMMC-7721 cells. (E) The expression of LC3-II was quantified by densitometry and normalized by β-actin. (F) Detection of ROS production by CM-H2DCFDA staining and flow cytometry analysis in SMMC-7721 cells infected with ZD55-vector or ZD55-IFN-β at 48 h post-infection. MOI = 2. Results are expressed as the mean ± SD from three separate experiments. $*P < 0.05$, $***P < 0.001$. NS, not significant.

demonstrated that a proportion of cells were undergoing necroptosis. Moreover, it was found that cellular LC3-II levels accumulated after ZD55-IFN-β infection, which was completely abolished by Nec-1 [**Fig. 4(D,E)**]. Importantly, the production of ROS which is essential for necroptosis was significantly increased at 24 h (data not shown) and 48 h after ZD55-IFN-β infection [**Fig. 4(F)**]. Taken together, these results demonstrated that ZD55-IFN-β induces both apoptosis and necroptosis in tumor cells.

Nec-1 converts ZD55-IFN-β-induced necroptosis to apoptosis

We further sought to determine the relationship between these two types of programmed cell death. To distinguish necroptosis from apoptosis, cells which were stained with PI with fragmented nuclei were regarded as apoptosis and the round cells were considered to be necroptosis. It was found that ZD55-IFN-β induced much more necrotic cell death (64%) than apoptotic cell death (36%) in SMMC-7721 cells at 48 h post-infection. In contrast, when cells were pre-treated with Nec-1, the percentage of necroptotic cells significantly reduced, whereas the percentage of apoptotic cells increased [**Fig. 5(A,B)**]. Because of relatively less membrane damage, apoptotic cells take up PI much more slowly than necrotic cells. Therefore, healthy (PI-negative), apoptotic (PI-dim), and necrotic (PI-bright) cells could be differentiated by flow cytometry. With Nec-1 pre-treatment, the PI-bright population was diminished from 25.32% to 9.83%, and PI-dim cells were slightly increased from 11.54% to 17.53%, supporting the idea that Nec-1 can efficiently convert the PI-bright cells (necroptosis) to PI-dim cells (apoptosis) [**Fig. 5(C,D)**]. Our data suggested that ZD55-IFN-β-induced necroptosis can be converted to apoptosis in the presence of Nec-1.

ZD55-IFN-β in combination with doxorubicin shows a synergistic effect

Many studies have demonstrated that dysregulation of the apoptotic machinery plays an important role in resistance to cancer drugs [27] we next tested the anti-tumor effect of

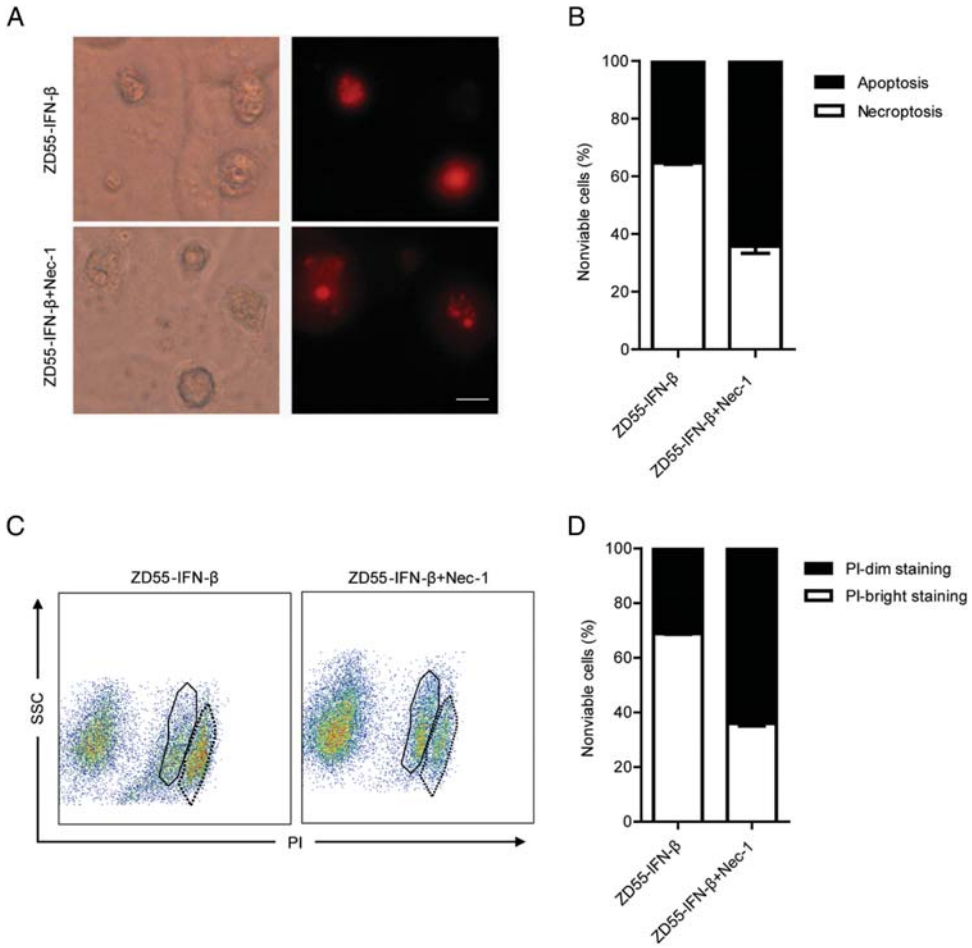

Figure 5 Nec-1 converts ZD55-IFN-β-induced necroptosis to apoptosis (A) Representative nuclear morphology of SMMC-7721 cells infected with ZD55-IFN-β in the presence or absence of Nec-1 and stained with PI. Left panel, phase contrast field; Right panel, fluorescence image. Scar bar = 20 μm. (B) Quantification of cells with fragmented nuclei (considered apoptotic cells) and cells with round nuclei (considered necroptotic cells) at 48 h after infected with ZD55-IFN-β in the presence or absence of Nec-1. (C) PI staining of SMMC-7721 cells at 48 h after infected with ZD55-IFN-β in the presence or absence of Nec-1. Healthy, apoptotic and necrotic cells showed PI-negative, PI-dim, and PI-bright staining, respectively. PI-bright cells are outlined with dotted lines and PI-dim cells are outlined with solid lines. Note that side-scattered light (SSC) is proportional to cell granularity or internal complexity (D) Quantification of PI-dim and PI-bright cells after treatment with ZD55-IFN-β or ZD55-IFN-β plus Nec-1.

the combination of ZD55-IFN-β and doxorubicin. Thus, SMMC-7721 cells were infected with ZD55-IFN-β at a multiplicity of infection (MOI) of 0.781, 1.562, 3.125, 6.25, 12.5, 25, 50, or 100, treated with doxorubicin at doses of 0.039, 0.078, 0.156, 0.313, 0.625, 1.25, 2.5, or 5 mg/l or treated with a combination of ZD55-IFN-β and doxorubicin. As shown in the dose–response curves, the combination of ZD55-IFN-β and doxorubicin induced the highest anti-proliferative effect [**Fig. 6(A)**]. The dose and response parameters were then used to calculate IC_{50} value and CI by CalcuSyn V2.0. The IC_{50} for ZD55-IFN-β alone and doxorubicin alone was 972 MOI and 0.86 mg/l, respectively, but after combination, the IC_{50} for ZD55-IFN-β and doxorubicin was reduced to 6.73 MOI and 0.34 mg/l, respectively [**Fig. 6(A)**]. To assess the effect of the combination of ZD55-IFN-β and doxorubicin, the CI and improved IC_{50}-isobologram analyses were used to determinate synergism or antagonism. The CI value of ZD55-IFN-β and doxorubicin was <1, which meant that ZD55-IFN-β and doxorubicin had a synergistic effect on SMMC-7721 cells [**Fig. 6(B)**]. Consistent with the CI analysis, the experimental IC_{50} data points for the combination of ZD55-IFN-β and doxorubicin plotted below the envelope, which also indicated a synergistic effect [**Fig. 6(C)**]. Similar results could also be observed in human prostate cancer cell line DU-145 (**Supplementary Fig. S2**).

Discussion

In our previous study, we constructed an E1B-attenuated oncolytic adenovirus, ZD55-IFN-β, with the goal of determining the anti-tumor effects of IFN-β. Upon infection with ZD55-IFN-β, the proliferation of tumor cells, and the growth of tumor xenografts were significantly inhibited.

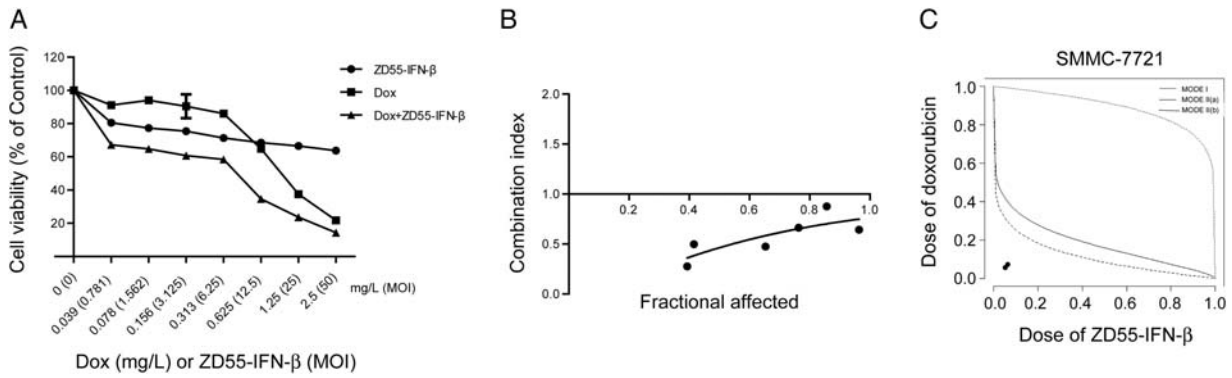

Figure 6 ZD55-IFN-β has a synergistic effect on SMMC-7721 cells when combined with doxorubicin (A) Dose-effect curves for SMMC-7721 cells after treatment with different combinations. Cell viability was determined by MTT assay. Uninfected cells were considered 100% viable. Points indicate mean values ($n = 6$). (B) CI vs. fraction-affected (fa) plots determined by the median-effect analysis program (CalcuSyn). Based on parameters (m and Dm values) for doxorubicin and ZD55-IFN-β combinations, the predicted fa-CI curves were drawn (solid line). Solid circles are actual combination data points. CI < 1 indicates synergism. (C) Isobologram analysis of the effects of doxorubicin combined with ZD55-IFN-β. Three isoeffect lines (mode I, mode IIa, and mode IIb) enclosing an 'envelope of additivity' were drawn as described in 'Materials and Methods'. Data points (•) were determined from the combination treatment experiments. When the experimental data points for the combination plot fell below the envelope, the combination was supra-additive (synergism).

These findings led us to investigate the underlying mechanisms of IFN-β-mediated cell death. Here, we fortuitously discovered that ZD55-IFN-β-induced S-phase arrest in SMMC-7721 cells via p53-dependent DNA damage pathway. Furthermore, ZD55-IFN-β was found to activate induced both apoptosis and necroptosis. Thus, we proposed a combination strategy to overcome cancer drug resistance and found that the combination of ZD55-IFN-β and doxorubicin had a synergistic effect on both SMMC-7721 and DU-145 cells, indicating that use of ZD55-IFN-β with other chemotherapy drugs could represent a promising combination strategy.

A question worth considering is the relationship between apoptosis and necroptosis, as both are induced by the overexpression of IFN-β. Because necroptosis was observed at the early stage after ZD55-IFN-β infection and blocking necroptosis by Nec-1 accelerated the apoptotic process, we propose that IFN-β-triggered necroptosis occurs before apoptosis and, ultimately, is replaced by apoptosis. Indeed, it has been reported that apoptosis supersedes programmed necrosis by degradation of RIP, which is the key molecule in the necroptotic process [28]. In addition, another study has indicated that intracellular ATP levels determine the type of cell death because incubation of cells under ATP-depleting conditions results in necrotic cell death and incubation of cells under ATP-enhanced conditions results in apoptotic cell death [29]. These findings strengthen our hypothesis that IFN-β-induced necroptosis can be replaced by apoptosis, which is further supported by the observation that cellular ATP levels sharply dropped at 24 h after ZD55-IFN-β infection but unexpectedly returned to normal at 48 h [**Fig. 4(B)**].

In the present study, we demonstrated that the overexpression of IFN-β gave rise to diverse cell death fates. It should be noted that only *in vitro* experiments were carried out here. The versatile function of ZD55-IFN-β requires further investigation *in vivo*, especially the ability of ZD55-IFN-β to reverse resistance to cancer drugs. Taken together, our findings showed that a conditionally replicative adenovirus carrying IFN-β not only induced S-phase arrest but also triggered both apoptosis and necroptosis in tumor cells. Thus, ZD55-IFN-β has a strong potential to reverse cancer drug resistance, and the combination of ZD55-IFN-β with doxorubicin may represent a promising clinical strategy in cancer therapy.

Supplementary data

Supplementary data are available at *ABBS* online.

Acknowledgements

We thank Prof Jian Ding (Shanghai Institute of Materia Medica, Shanghai, China) for providing p-ATM and p-Chk2 antibodies and Lanying Sun (Shanghai Institute of Biochemistry and Cell Biology, Shanghai, China) and Xuedong Wang (Shanghai Institute of Biochemistry and Cell Biology) for professional technical assistance.

Funding

This work was supported by the grants from the National Natural Science Foundation of China (30623003 and 81172449), National Basic Research Program of China (973 Program) (2010CB529901 and 2011CB510104),

Important National Science & Technology Specific Project of Hepatitis and Hepatoma Related Program (2008ZX10002–023), New Innovation Program (2009-ZX-09102–246), and Zhejiang Sci-Tech University grant (1016834-Y).

References

1 Parmar S and Platanias LC. Interferons: mechanisms of action and clinical applications. Curr Opin Oncol 2003, 15: 431–439.

2 Shimizu M, Akiyama S, Ito K, Kasai Y, Takagi H, Kito M and Ohishi N, *et al*. Effect on colon cancer cells of human interferon-beta gene entrapped in cationic multilamellar liposomes. Biochem Mol Biol Int 1998, 44: 1235–1243.

3 Qin XQ, Beckham C, Brown JL, Lukashev M and Barsoum J. Human and mouse IFN-beta gene therapy exhibits different anti-tumor mechanisms in mouse models. Mol Ther 2001, 4: 356–364.

4 Tough DF, Borrow P and Sprent J. Induction of bystander T cell proliferation by viruses and type I interferon *in vivo*. Science 1996, 272: 1947–1950.

5 Singh RK, Gutman M, Bucana CD, Sanchez R, Llansa N and Fidler IJ. Interferons alpha and beta down-regulate the expression of basic fibroblast growth factor in human carcinomas. Proc Natl Acad Sci USA 1995, 92: 4562–4566.

6 Qin XQ, Tao N, Dergay A, Moy P, Fawell S, Davis A and Wilson JM,, *et al*. Interferon-beta gene therapy inhibits tumor formation and causes regression of established tumors in immune-deficient mice. Proc Natl Acad Sci USA 1998, 95: 14411–14416.

7 Ravandi F, Estrov Z, Kurzrock R, Breitmeyer JB, Maschek BJ and Talpaz M. A phase I study of recombinant interferon-beta in patients with advanced malignant disease. Clin Cancer Res 1999, 5: 3990–3998.

8 He LF, Gu JF, Tang WH, Fan JK, Wei N, Zou WG and Zhang YH, *et al*. Significant antitumor activity of oncolytic adenovirus expressing human interferon-beta for hepatocellular carcinoma. J Gene Med 2008, 10: 983–992.

9 Gottesman MM. Mechanisms of cancer drug resistance. Annu Rev Med 2002, 53: 615–627.

10 Han W, Li L, Qiu S, Lu Q, Pan Q, Gu Y and Luo J, *et al*. Shikonin circumvents cancer drug resistance by induction of a necroptotic death. Mol Cancer Ther 2007, 6: 1641–1649.

11 Hu X and Xuan Y. Bypassing cancer drug resistance by activating multiple death pathways—a proposal from the study of circumventing cancer drug resistance by induction of necroptosis. Cancer Lett 2008, 259: 127–137.

12 Degterev A and Yuan J. Expansion and evolution of cell death programmes. Nat Rev Mol Cell Biol 2008, 9: 378–390.

13 Degterev A, Huang Z, Boyce M, Li Y, Jagtap P, Mizushima N and Cuny GD, *et al*. Chemical inhibitor of nonapoptotic cell death with therapeutic potential for ischemic brain injury. Nat Chem Biol 2005, 1: 112–119.

14 Asare N, Lag M, Lagadic-Gossmann D, Rissel M, Schwarze P and Holme JA. 3-Nitrofluoranthene (3-NF) but not 3-aminofluoranthene (3-AF) elicits apoptosis as well as programmed necrosis in Hepa1c1c7 cells. Toxicology 2009, 255: 140–150.

15 Li Y, Yang X, Ma C, Qiao J and Zhang C. Necroptosis contributes to the NMDA-induced excitotoxicity in rat's cultured cortical neurons. Neurosci Lett 2008, 447: 120–123.

16 Aoe K, Kiura K, Ueoka H, Tabata M, Matsumura T, Chikamori M and Matsushita A, *et al*. Effect of docetaxel with cisplatin or vinorelbine on lung cancer cell lines. Anticancer Res 1999, 19: 291–299.

17 Vitale M, Zauli Z and Falcieri E. APOPTOSIS vs. NECROSIS. The Purdue Cytometry CD-ROM. Volume 4. 1998.

18 Darzynkiewicz Z, Juan G, Li X, Gorczyca W, Murakami T and Traganos F. Cytometry in cell necrobiology: analysis of apoptosis and accidental cell death (necrosis). Cytometry 1997, 27: 1–20.

19 Vitale M, Zamai L, Mazzotti G, Cataldi A and Falcieri E. Differential kinetics of propidium iodide uptake in apoptotic and necrotic thymocytes. Histochemistry 1993, 100: 223–229.

20 Sato T, Machida T, Takahashi S, Murase K, Kawano Y, Hayashi T and Iyama S, *et al*. Apoptosis supercedes necrosis in mitochondrial DNA-depleted Jurkat cells by cleavage of receptor-interacting protein and inhibition of lysosomal cathepsin. J Immunol 2008, 181: 197–207.

21 Radhakrishnan SK, Feliciano CS, Najmabadi F, Haegebarth A, Kandel ES, Tyner AL and Gartel AL. Constitutive expression of E2F-1 leads to p21-dependent cell cycle arrest in S phase of the cell cycle. Oncogene 2004, 23: 4173–4176.

22 Zhang Y, Rishi AK, Dawson MI, Tschang R, Farhana L, Boyanapalli M and Reichert U, *et al*. S-phase arrest and apoptosis induced in normal mammary epithelial cells by a novel retinoid. Cancer Res 2000, 60: 2025–2032.

23 Morgan SE and Kastan MB. p53 and ATM: cell cycle, cell death, and cancer. Adv Cancer Res 1997, 71: 1–25.

24 Bendjennat M, Boulaire J, Jascur T, Brickner H, Barbier V, Sarasin A and Fotedar A, *et al*. UV irradiation triggers ubiquitin-dependent degradation of p21(WAF1) to promote DNA repair. Cell 2003, 114: 599–610.

25 Horita H, Frankel AE and Thorburn A. Acute myeloid leukemia-targeted toxin activates both apoptotic and necroptotic death mechanisms. PLoS One 2008, 3: e3909.

26 Kroemer G, Galluzzi L, Vandenabeele P, Abrams J, Alnemri ES, Baehrecke EH and Blagosklonny MV, *et al*. Classification of cell death: recommendations of the Nomenclature Committee on Cell Death 2009. Cell Death Differ 2009, 16: 3–11.

27 Yague E and Raguz S. Drug resistance in cancer. Br J Cancer 2005, 93: 973–976.

28 Zhang DW, Shao J, Lin J, Zhang N, Lu BJ, Lin SC and Dong MQ, *et al*. RIP3, an energy metabolism regulator that switches TNF-induced cell death from apoptosis to necrosis. Science 2009, 325: 332–336.

29 Eguchi Y, Shimizu S and Tsujimoto Y. Intracellular ATP levels determine cell death fate by apoptosis or necrosis. Cancer Res 1997, 57: 1835–1840.